BELLE-CONF-0557
LP2005-192
EPS05-532

Hadronic Mass Moments in $B \to X_c \ell \nu$ Decays

K. Abe,[9] K. Abe,[47] I. Adachi,[9] H. Aihara,[49] K. Aoki,[23] K. Arinstein,[2] Y. Asano,[54] T. Aso,[53] V. Aulchenko,[2] T. Aushev,[13] T. Aziz,[45] S. Bahinipati,[5] A. M. Bakich,[44] V. Balagura,[13] Y. Ban,[36] S. Banerjee,[45] E. Barberio,[22] M. Barbero,[8] A. Bay,[19] I. Bedny,[2] U. Bitenc,[14] I. Bizjak,[14] S. Blyth,[25] A. Bondar,[2] A. Bozek,[29] M. Bračko,[9,21,14] J. Brodzicka,[29] T. E. Browder,[8] M.-C. Chang,[48] P. Chang,[28] Y. Chao,[28] A. Chen,[25] K.-F. Chen,[28] W. T. Chen,[25] B. G. Cheon,[4] C.-C. Chiang,[28] R. Chistov,[13] S.-K. Choi,[7] Y. Choi,[43] Y. K. Choi,[43] A. Chuvikov,[37] S. Cole,[44] J. Dalseno,[22] M. Danilov,[13] M. Dash,[56] L. Y. Dong,[11] R. Dowd,[22] J. Dragic,[9] A. Drutskoy,[5] S. Eidelman,[2] Y. Enari,[23] D. Epifanov,[2] F. Fang,[8] S. Fratina,[14] H. Fujii,[9] N. Gabyshev,[2] A. Garmash,[37] T. Gershon,[9] A. Go,[25] G. Gokhroo,[45] P. Goldenzweig,[5] B. Golob,[20,14] A. Gorišek,[14] M. Grosse Perdekamp,[38] H. Guler,[8] R. Guo,[26] J. Haba,[9] K. Hara,[9] T. Hara,[34] Y. Hasegawa,[42] N. C. Hastings,[49] K. Hasuko,[38] K. Hayasaka,[23] H. Hayashii,[24] M. Hazumi,[9] T. Higuchi,[9] L. Hinz,[19] T. Hojo,[34] T. Hokuue,[23] Y. Hoshi,[47] K. Hoshina,[52] S. Hou,[25] W.-S. Hou,[28] Y. B. Hsiung,[28] Y. Igarashi,[9] T. Iijima,[23] K. Ikado,[23] A. Imoto,[24] K. Inami,[23] A. Ishikawa,[9] H. Ishino,[50] K. Itoh,[49] R. Itoh,[9] M. Iwasaki,[49] Y. Iwasaki,[9] C. Jacoby,[19] C.-M. Jen,[28] R. Kagan,[13] H. Kakuno,[49] J. H. Kang,[57] J. S. Kang,[16] P. Kapusta,[29] S. U. Kataoka,[24] N. Katayama,[9] H. Kawai,[3] N. Kawamura,[1] T. Kawasaki,[31] S. Kazi,[5] N. Kent,[8] H. R. Khan,[50] A. Kibayashi,[50] H. Kichimi,[9] H. J. Kim,[18] H. O. Kim,[43] J. H. Kim,[43] S. K. Kim,[41] S. M. Kim,[43] T. H. Kim,[57] K. Kinoshita,[5] N. Kishimoto,[23] S. Korpar,[21,14] Y. Kozakai,[23] P. Križan,[20,14] P. Krokovny,[9] T. Kubota,[23] R. Kulasiri,[5] C. C. Kuo,[25] H. Kurashiro,[50] E. Kurihara,[3] A. Kusaka,[49] A. Kuzmin,[2] Y.-J. Kwon,[57] J. S. Lange,[6] G. Leder,[12] S. E. Lee,[41] Y.-J. Lee,[28] T. Lesiak,[29] J. Li,[40] A. Limosani,[9] S.-W. Lin,[28] D. Liventsev,[13] J. MacNaughton,[12] G. Majumder,[45] F. Mandl,[12] D. Marlow,[37] H. Matsumoto,[31] T. Matsumoto,[51] A. Matyja,[29] Y. Mikami,[48] W. Mitaroff,[12] K. Miyabayashi,[24] H. Miyake,[34] H. Miyata,[31] Y. Miyazaki,[23] R. Mizuk,[13] D. Mohapatra,[56] G. R. Moloney,[22] T. Mori,[50] A. Murakami,[39] T. Nagamine,[48] Y. Nagasaka,[10] T. Nakagawa,[51] I. Nakamura,[9] E. Nakano,[33] M. Nakao,[9] H. Nakazawa,[9] Z. Natkaniec,[29] K. Neichi,[47] S. Nishida,[9] O. Nitoh,[52] S. Noguchi,[24] T. Nozaki,[9] A. Ogawa,[38] S. Ogawa,[46] T. Ohshima,[23] T. Okabe,[23] S. Okuno,[15] S. L. Olsen,[8] Y. Onuki,[31] W. Ostrowicz,[29] H. Ozaki,[9] P. Pakhlov,[13] H. Palka,[29] C. W. Park,[43] H. Park,[18] K. S. Park,[43] N. Parslow,[44] L. S. Peak,[44] M. Pernicka,[12] R. Pestotnik,[14] M. Peters,[8] L. E. Piilonen,[56] A. Poluektov,[2] F. J. Ronga,[9] N. Root,[2] M. Rozanska,[29] H. Sahoo,[8] M. Saigo,[48] S. Saitoh,[9] Y. Sakai,[9] H. Sakamoto,[17] H. Sakaue,[33] T. R. Sarangi,[9] M. Satapathy,[55] N. Sato,[23] N. Satoyama,[42] T. Schietinger,[19] O. Schneider,[19] P. Schönmeier,[48] J. Schümann,[28] C. Schwanda,[12] A. J. Schwartz,[5] T. Seki,[51] K. Senyo,[23] R. Seuster,[8] M. E. Sevior,[22] T. Shibata,[31] H. Shibuya,[46] J.-G. Shiu,[28] B. Shwartz,[2] V. Sidorov,[2] J. B. Singh,[35] A. Somov,[5] N. Soni,[35] R. Stamen,[9] S. Stanič,[32] M. Starič,[14] A. Sugiyama,[39] K. Sumisawa,[9] T. Sumiyoshi,[51] S. Suzuki,[39] S. Y. Suzuki,[9] O. Tajima,[9] N. Takada,[42] F. Takasaki,[9] K. Tamai,[9] N. Tamura,[31] K. Tanabe,[49] M. Tanaka,[9] G. N. Taylor,[22] Y. Teramoto,[33] X. C. Tian,[36] K. Trabelsi,[8] Y. F. Tse,[22] T. Tsuboyama,[9] T. Tsukamoto,[9] K. Uchida,[8] Y. Uchida,[9] S. Uehara,[9]

T. Uglov,[13] K. Ueno,[28] Y. Unno,[9] S. Uno,[9] P. Urquijo,[22] Y. Ushiroda,[9] G. Varner,[8] K. E. Varvell,[44] S. Villa,[19] C. C. Wang,[28] C. H. Wang,[27] M.-Z. Wang,[28] M. Watanabe,[31] Y. Watanabe,[50] L. Widhalm,[12] C.-H. Wu,[28] Q. L. Xie,[11] B. D. Yabsley,[56] A. Yamaguchi,[48] H. Yamamoto,[48] S. Yamamoto,[51] Y. Yamashita,[30] M. Yamauchi,[9] Heyoung Yang,[41] J. Ying,[36] S. Yoshino,[23] Y. Yuan,[11] Y. Yusa,[48] H. Yuta,[1] S. L. Zang,[11] C. C. Zhang,[11] J. Zhang,[9] L. M. Zhang,[40] Z. P. Zhang,[40] V. Zhilich,[2] T. Ziegler,[37] and D. Zürcher[19]

(The Belle Collaboration)

[1]*Aomori University, Aomori*
[2]*Budker Institute of Nuclear Physics, Novosibirsk*
[3]*Chiba University, Chiba*
[4]*Chonnam National University, Kwangju*
[5]*University of Cincinnati, Cincinnati, Ohio 45221*
[6]*University of Frankfurt, Frankfurt*
[7]*Gyeongsang National University, Chinju*
[8]*University of Hawaii, Honolulu, Hawaii 96822*
[9]*High Energy Accelerator Research Organization (KEK), Tsukuba*
[10]*Hiroshima Institute of Technology, Hiroshima*
[11]*Institute of High Energy Physics, Chinese Academy of Sciences, Beijing*
[12]*Institute of High Energy Physics, Vienna*
[13]*Institute for Theoretical and Experimental Physics, Moscow*
[14]*J. Stefan Institute, Ljubljana*
[15]*Kanagawa University, Yokohama*
[16]*Korea University, Seoul*
[17]*Kyoto University, Kyoto*
[18]*Kyungpook National University, Taegu*
[19]*Swiss Federal Institute of Technology of Lausanne, EPFL, Lausanne*
[20]*University of Ljubljana, Ljubljana*
[21]*University of Maribor, Maribor*
[22]*University of Melbourne, Victoria*
[23]*Nagoya University, Nagoya*
[24]*Nara Women's University, Nara*
[25]*National Central University, Chung-li*
[26]*National Kaohsiung Normal University, Kaohsiung*
[27]*National United University, Miao Li*
[28]*Department of Physics, National Taiwan University, Taipei*
[29]*H. Niewodniczanski Institute of Nuclear Physics, Krakow*
[30]*Nippon Dental University, Niigata*
[31]*Niigata University, Niigata*
[32]*Nova Gorica Polytechnic, Nova Gorica*
[33]*Osaka City University, Osaka*
[34]*Osaka University, Osaka*
[35]*Panjab University, Chandigarh*
[36]*Peking University, Beijing*
[37]*Princeton University, Princeton, New Jersey 08544*
[38]*RIKEN BNL Research Center, Upton, New York 11973*

[39]Saga University, Saga
[40]University of Science and Technology of China, Hefei
[41]Seoul National University, Seoul
[42]Shinshu University, Nagano
[43]Sungkyunkwan University, Suwon
[44]University of Sydney, Sydney NSW
[45]Tata Institute of Fundamental Research, Bombay
[46]Toho University, Funabashi
[47]Tohoku Gakuin University, Tagajo
[48]Tohoku University, Sendai
[49]Department of Physics, University of Tokyo, Tokyo
[50]Tokyo Institute of Technology, Tokyo
[51]Tokyo Metropolitan University, Tokyo
[52]Tokyo University of Agriculture and Technology, Tokyo
[53]Toyama National College of Maritime Technology, Toyama
[54]University of Tsukuba, Tsukuba
[55]Utkal University, Bhubaneswer
[56]Virginia Polytechnic Institute and State University, Blacksburg, Virginia 24061
[57]Yonsei University, Seoul

Abstract

We report measurements of the first and second moments of the hadronic invariant mass squared distribution, $\langle M_X^2 \rangle$ and $\langle (M_X^2 - \langle M_X^2 \rangle)^2 \rangle$, in $B \to X_c \ell \nu$ decays for minimum lepton momenta ranging from 0.7 to 1.5 GeV/c in the B meson rest frame. The measurement uses $B\bar{B}$ events in which the hadronic decay of one B meson is fully reconstructed and the semileptonic decay of the other B is inferred from the presence of an identified lepton. These results are obtained from a 140 fb^{-1} data sample collected near the $\Upsilon(4S)$ resonance with the Belle detector at the KEKB asymmetric energy e^+e^- collider.

Recently, there have been intense theoretical and experimental efforts toward predicting [1, 2, 3, 4] and measuring [5, 6, 7] the moments of the hadronic invariant mass squared distribution in $B \to X_c \ell \nu$ decays. The idea is that using the Operator Product Expansion (OPE) [8], the hadronic mass moments (and other inclusive observables in B decays) can be predicted in terms of the b-quark mass m_b and other non-perturbative parameters. Conversely, by measuring the moments of B decay spectra and the semileptonic B decay rate, one can then extract these parameters and $|V_{cb}|$ [9].

The analysis is based on the data recorded with the Belle detector [10] at the asymmetric energy e^+e^- collider KEKB [11], operating at a center-of-mass (c.m.) energy near the $\Upsilon(4S)$ resonance. KEKB consists of a low energy ring (LER) of 3.5 GeV positrons and a high energy ring (HER) of 8 GeV electrons. The Belle detector is a large-solid-angle magnetic spectrometer consisting of a three-layer silicon vertex detector (SVD), a 50-layer central drift chamber (CDC), an array of aerogel threshold Čerenkov counters (ACC), a barrel-like arrangement of time-of-flight scintillation counters (TOF), and an electromagnetic calorimeter comprised of CsI(Tl) crystals (ECL) located inside a super-conducting solenoid coil that provides a 1.5 T magnetic field. The responses of the ECL, CDC (dE/dx) and ACC detectors are combined to provide clean electron identification. Muons are identified in the instrumented iron flux-return (KLM) located outside of the coil. Charged hadron identification relies on the information from the CDC, ACC and TOF sub-detectors.

The $\Upsilon(4S)$ dataset used for this study corresponds to an integrated luminosity of 140 fb^{-1}, or about 152 million $B\bar{B}$ events. Another 15 fb^{-1} taken 60 MeV below the resonance are used to subtract the non-$B\bar{B}$ (continuum) background. Full detector simulation based on GEANT [12] is applied to Monte Carlo (MC) simulated events. The size of the MC samples is equivalent to about 2.4 times the integrated luminosity. At the generator level, the decay $B \to D^* \ell \nu$ is simulated using a HQET-based model [13]. The ISGW2 model [14] is used for the decays $B \to D \ell \nu$ and $B \to D^{**} \ell \nu$. The non-resonant $B \to D^{(*)} \pi \ell \nu$ component is generated according to the model of Goity and Roberts [15]. QED bremsstrahlung in semileptonic decays is simulated by the PHOTOS package [16].

After selecting hadronic events [17], we fully reconstruct the hadronic decay of one B meson ($B_{\rm tag}$) using the decay modes $B^+ \to \bar{D}^{(*)0}\pi^+, \bar{D}^{(*)0}\rho^+, \bar{D}^{(*)0}a_1^+$ and $B^0 \to D^{(*)-}\pi^+, D^{(*)-}\rho^+, D^{(*)-}a_1^+$ [18]. Pairs of photons satisfying $E_\gamma > 50$ MeV and $117\ {\rm MeV}/c^2 < m(\gamma\gamma) < 150\ {\rm MeV}/c^2$ are combined to form π^0 candidates. K^0_S mesons are reconstructed from pairs of oppositely charged tracks with invariant mass within $\pm 30\ {\rm MeV}/c^2$ of the K^0_S mass and decay vertex displaced from the interaction point. Candidate ρ^+ and ρ^0 mesons are reconstructed in the $\pi^+\pi^0$ and $\pi^+\pi^-$ decay modes, requiring their invariant masses to be within $\pm 150\ {\rm MeV}/c^2$ of the ρ mass. Candidate a_1^+ mesons are obtained by combining a ρ^0 candidate with a charged pion and requiring an invariant mass between 1.0 and 1.6 GeV/c^2. D^0 candidates are searched for in the $K^-\pi^+$, $K^-\pi^+\pi^0$, $K^-\pi^+\pi^+\pi^-$, $K^0_S\pi^+\pi^-$ and $K^0_S\pi^0$ decay modes. The $K^-\pi^+\pi^+$ and $K^0_S\pi^+$ modes are used to reconstruct D^+ mesons. Charmed mesons are selected in a window corresponding to ± 3 times the mass resolution in the respective decay mode. D^{*+} mesons are reconstructed by pairing a charmed meson with a low momentum pion, $D^{*+} \to D^0\pi^+, D^+\pi^0$. The decay modes $D^{*0} \to D^0\pi^0$ and $D^{*0} \to D^0\gamma$ are used to search for neutral charmed vector mesons.

For each $B_{\rm tag}$ candidate, the beam-constrained mass $M_{\rm bc}$ and the energy difference ΔE are calculated

$$M_{\rm bc} = \sqrt{(E_{\rm beam})^2 - (\vec{p}_B)^2}\ , \quad \Delta E = E_B - E_{\rm beam}\ , \tag{1}$$

where $E_{\rm beam}$ is the beam energy in the c.m. system and $\vec{p}_B$ and E_B are the 3-momentum and

the energy of the $B_{\rm tag}$ candidate in the same frame, respectively. The signal region for $B_{\rm tag}$ is defined by the selections $M_{\rm bc} > 5.27$ GeV/c^2 and $|\Delta E| < 50$ MeV. If multiple candidates are found in a single event, the best candidate is chosen based on ΔE and other variables.

Semileptonic decays of the other B meson ($B_{\rm signal}$) are selected by searching for an identified charged lepton (electron or muon) within the remaining particles in the event. Events with multiple identified leptons are rejected. In the lepton momentum range relevant to this analysis, electrons (muons) are selected with an efficiency of 92% (89%) and the probability to misidentify a pion as an electron (a muon) is 0.25% (1.4%) [19, 20]. For B^+ tags, we require that the lepton has a charge sign compatible with a prompt semileptonic decay ($Q_\ell \cdot Q_B < 0$, where Q_ℓ and Q_B are the charges of the lepton and of $B_{\rm tag}$, respectively). In electron events, we attempt to recover bremsstrahlung photons by searching for a $E_\gamma < 1$ GeV photon within a 5° cone with respect to the electron direction. If such a photon is found, it is merged with the reconstructed electron candidate.

Charged and neutral particles in the event associated neither with $B_{\rm tag}$ nor with the charged lepton are assigned to the hadronic X system. The missing 4-momentum in the event is calculated, assigning the pion mass to all charged particles except identified kaons,

$$p_{\rm miss} = (p_{\rm LER} + p_{\rm HER}) - p_{B_{\rm tag}} - p_\ell - p_X \ , \tag{2}$$

where the indices LER and HER refer to the colliding beams. As only the neutrino in $B \to X_c \ell \nu$ should be missing in the event, the missing mass is required to be consistent with zero, $|M^2_{\rm miss}| < 3$ GeV$^2/c^4$. To improve the resolution in M_X^2, we constrain the neutrino mass to zero, $p_\nu = (|\vec{p}_{\rm miss}|, \vec{p}_{\rm miss})$, and recalculate the 4-momentum of the X system,

$$p'_X = (p_{\rm LER} + p_{\rm HER}) - p_{B_{\rm tag}} - p_\ell - p_\nu \ . \tag{3}$$

The M_X^2 resolution (defined as half width at the half maximum) obtained in this way is about 800 MeV$^2/c^4$.

For the rest of the analysis, the remaining events are divided into four sub-samples, depending on the charge of $B_{\rm tag}$ (B^+, B^0) and on the lepton type (electron, muon). In each of these sub-samples and for each lepton momentum threshold considered in the analysis ($p^*_\ell > 0.7$, 0.9, 1.1, 1.3 and 1.5 GeV/c [21]), the backgrounds in the M_X^2 distribution are determined, taking into account contributions from the following sources: continuum background, $B\bar{B}$ events with a misreconstructed $B_{\rm tag}$ candidate, and background from secondary or fake leptons. The background shapes in M_X^2 are determined from the MC simulation, except for the continuum where the off-resonance data is used. The shape of the fake muon background is corrected by the ratio of the pion fake rate in the experimental data over the same quantity in the MC simulation, as measured using $K^0_S \to \pi^+\pi^-$ decays. The continuum background is scaled by the on- to off-resonance luminosity ratio, taking into account the cross-section difference. The combinatorial $B_{\rm tag}$ background is normalized using the 5.20 GeV/$c^2 < M_{\rm bc} <$ 5.25 GeV/c^2 sideband. The normalization of the secondary or fake lepton background is found from the real data by fitting the lepton momentum distribution. The purity of the $B \to X_c \ell \nu$ signal depends on the sub-sample and the lepton momentum threshold, typical values being around 75%. Table I shows the numbers of signal events and purities for each combination of $B_{\rm tag}$ charge, lepton type and lepton momentum threshold.

In each of the four sub-samples and for each lepton momentum threshold, the M_X^2 distribution is measured in 39 bins in the range from 0 to 13 GeV$^2/c^4$ (bin width 0.333 GeV$^2/c^4$) and, after subtraction of all backgrounds, the finite detector resolution in M_X^2 is unfolded using the Singular Value Decomposition (SVD) algorithm [22], as illustrated in Fig. 1. The

$p^*_{\rm min}$	B^+ electron	B^+ muon	B^0 electron	B^0 muon
0.7	3893 ± 79 (72.3%)	3626 ± 84 (68.7%)	2212 ± 64 (66.4%)	2154 ± 64 (65.0%)
0.9	3659 ± 75 (74.0%)	3484 ± 78 (71.1%)	2072 ± 58 (66.4%)	2067 ± 58 (70.2%)
1.1	3285 ± 70 (75.2%)	3159 ± 73 (72.9%)	1886 ± 53 (66.4%)	1925 ± 52 (76.1%)
1.3	2742 ± 64 (75.9%)	2740 ± 66 (75.0%)	1595 ± 46 (66.4%)	1632 ± 47 (79.4%)
1.5	2152 ± 56 (77.7%)	2132 ± 56 (76.8%)	1195 ± 39 (66.4%)	1297 ± 41 (83.0%)

TABLE I: Number of $B \to X_c \ell \nu$ signal and signal purity in the four sub-samples, as a function of the lepton momentum threshold. The yields are quoted with their statistical uncertainty; the corresponding signal purity is given in brackets.

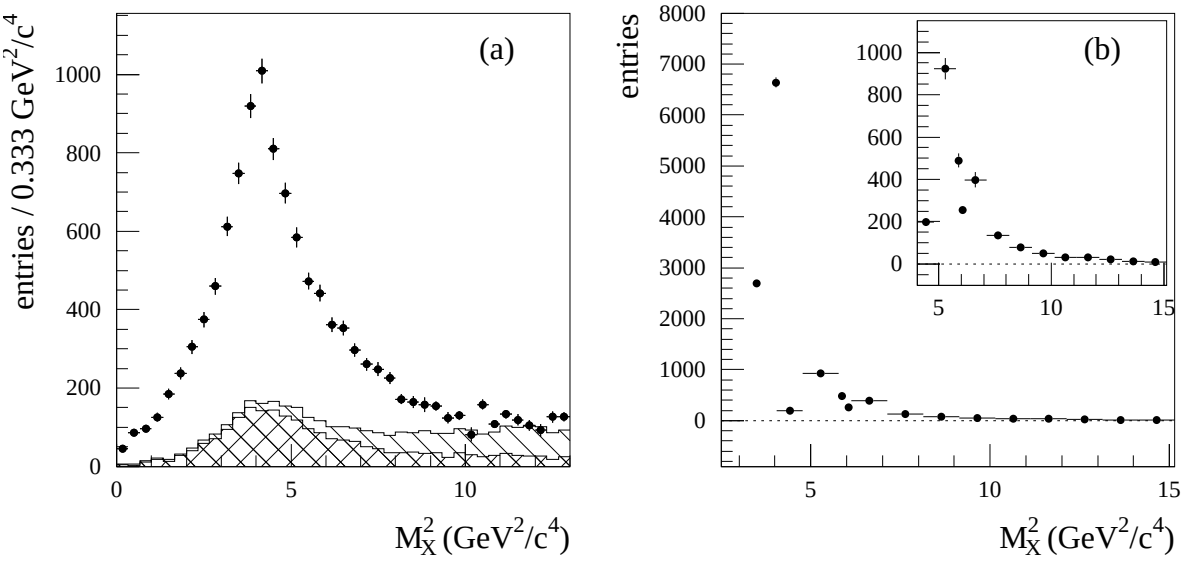

FIG. 1: (a) Measured and (b) unfolded M_X^2 distribution for $p_\ell^* > 0.7$ GeV/c. On the left plot, the continuum-subtracted M_X^2 distribution is shown by points with error bars. The hatched histogram corresponds to the background from secondary or fake leptons; $B\bar{B}$ events in which $B_{\rm tag}$ is misreconstructed are shown by the double-hatched histogram. The right plot is the result of the unfolding. In both plots, contributions from B^+ and B^0 tags, and from electron and muon events are added.

unfolded distribution has 15 bins in the range from M_D^2 to about 15 GeV$^2/c^4$ (bin width 1 GeV$^2/c^4$, except around the narrow states D, D^*, D_1 and D_2^*). We calculate the first and second moment, $\langle M_X^2 \rangle$ and $\langle (M_X^2 - \langle M_X^2 \rangle)^2 \rangle$, for each unfolded M_X^2 spectrum separately, after applying a small correction for different bin-to-bin efficiencies. The final results for a given lepton momentum threshold are obtained by taking the average over the four subsamples. The unfolding, moment calculation and averaging procedure has been studied on MC simulated events and no significant bias has been found.

The results for the first and second hadronic mass moment are shown in Fig. 2 and Tables II and III. All results are preliminary. Note that the moment measurements for different lepton momentum thresholds are highly correlated due to overlapping data samples.

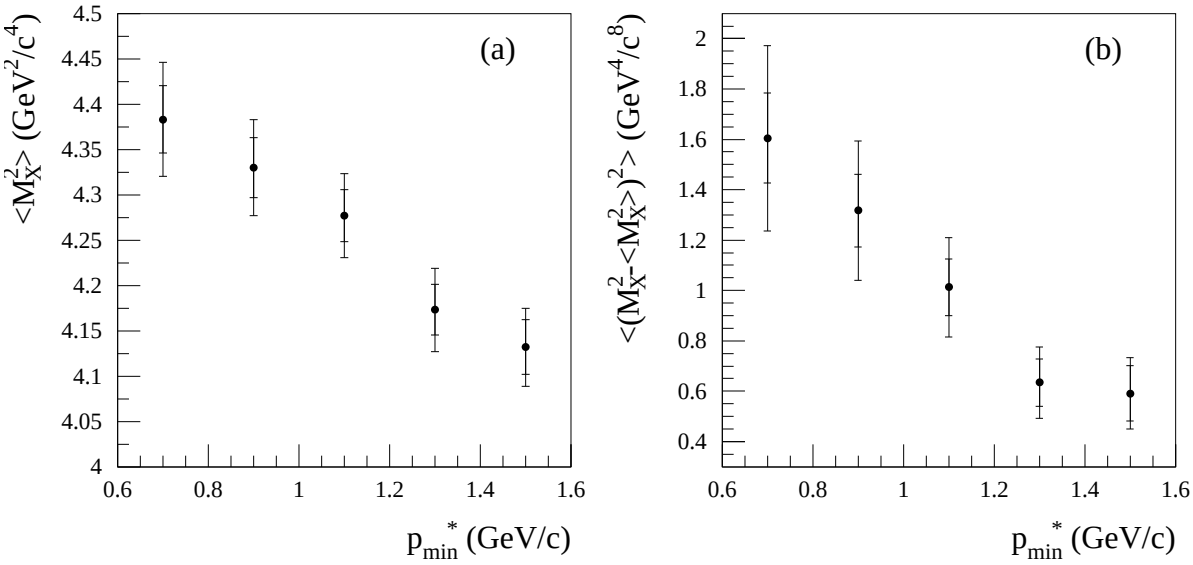

FIG. 2: (a) First and (b) second hadronic mass moment, $\langle M_X^2 \rangle$ and $\langle (M_X^2 - \langle M_X^2 \rangle)^2 \rangle$, for different lepton threshold momenta. The error bars indicate the statistical and total errors. Note that the individual moments are highly correlated. All results are preliminary.

$p^*_{\rm min}$ (GeV/c)	$\langle M_X^2 \rangle$ (GeV$^2/c^4$)	detector/ background	unfolding	X_c model
0.7	$4.383 \pm 0.037 \pm 0.051$	0.047	0.004	0.020
0.9	$4.330 \pm 0.033 \pm 0.041$	0.036	0.009	0.018
1.1	$4.277 \pm 0.029 \pm 0.035$	0.028	0.014	0.016
1.3	$4.173 \pm 0.028 \pm 0.037$	0.026	0.021	0.016
1.5	$4.132 \pm 0.030 \pm 0.031$	0.019	0.018	0.016

TABLE II: First hadronic mass moment $\langle M_X^2 \rangle$ for different lepton threshold momenta. The first error on $\langle M_X^2 \rangle$ is statistical and the second is the estimated systematic uncertainty. The right-most three columns show the different components of the systematic error. All results are preliminary.

We have estimated the correlations due to this overlap in Table IV.

We consider three sources of systematic error, shown separately in columns three to five of Tables II and III: the uncertainty related to the detector modeling and the background subtraction, the uncertainty related to unfolding and the moment extraction procedure, and the uncertainty related to the X_c model in the MC simulation. The total systematic error is the quadratic sum of these three components.

The uncertainty related to the detector modeling and the background subtraction is estimated by varying the normalizations of the different background components and some of the selections used in the analysis (namely the $B_{\rm tag}$ signal region and the requirement on $M^2_{\rm miss}$). The uncertainty related to unfolding and moment extraction is obtained by varying the effective rank parameter in the SVD algorithm, dis- and enabling the bin-to-bin efficiency

$p^*_{\rm min}$ (GeV/c)	$\langle (M_X^2 - \langle M_X^2 \rangle)^2 \rangle$ (GeV$^4/c^8$)	detector/ background	unfolding	X_c model
0.7	$1.605 \pm 0.179 \pm 0.322$	0.233	0.184	0.123
0.9	$1.317 \pm 0.144 \pm 0.236$	0.174	0.116	0.110
1.1	$1.013 \pm 0.113 \pm 0.161$	0.125	0.047	0.089
1.3	$0.634 \pm 0.095 \pm 0.105$	0.079	0.028	0.064
1.5	$0.591 \pm 0.110 \pm 0.088$	0.035	0.068	0.043

TABLE III: Same as Table II for the second hadronic mass moment $\langle (M_X^2 - \langle M_X^2 \rangle)^2 \rangle$.

$p^*_{\rm min}$ (GeV/c)		$\langle M_X^2 \rangle$					$\langle (M_X^2 - \langle M_X^2 \rangle)^2 \rangle$				
		0.7	0.9	1.1	1.3	1.5	0.7	0.9	1.1	1.3	1.5
$\langle M_X^2 \rangle$	0.7	1.000	0.922	0.807	0.620	0.533	0.782	0.720	0.622	0.471	0.415
	0.9		1.000	0.875	0.672	0.579	0.705	0.781	0.674	0.511	0.450
	1.1			1.000	0.768	0.661	0.561	0.622	0.770	0.583	0.514
	1.3				1.000	0.861	0.347	0.384	0.476	0.759	0.670
	1.5					1.000	0.342	0.379	0.470	0.749	0.778
$\langle (M_X^2 - \langle M_X^2 \rangle)^2 \rangle$	0.7						1.000	0.902	0.728	0.456	0.440
	0.9							1.000	0.807	0.506	0.487
	1.1								1.000	0.627	0.603
	1.3									1.000	0.963
	1.5										1.000

TABLE IV: Estimated correlation coefficients for the different moment measurements due to overlapping data samples.

correction and changing the binning of the unfolded distribution. The X_c model uncertainty is determined by varying the fractions of $B \to D^* \ell\nu$, $B \to D \ell\nu$ and $B \to D^{**}/D^{(*)}\pi\ell\nu$ within $\pm 10\%$, $\pm 10\%$ and $\pm 30\%$, respectively, and summing the individual variations in quadrature. These ranges of variation roughly correspond to the experimental uncertainties [23] in the isospin averaged branching ratios.

In summary, we have measured the first and second moments of the hadronic invariant mass squared distribution, $\langle M_X^2 \rangle$ and $\langle (M_X^2 - \langle M_X^2 \rangle)^2 \rangle$, in $B \to X_c \ell\nu$ decays for minimum lepton momenta ranging from 0.7 to 1.5 GeV/c in the B rest frame. The results obtained are compatible with theoretical expectations [1] and recent measurements from other experiments [6, 7]. In addition, we have estimated the correlations of the moment measurements. These measurements can be used as input to a global fit analysis, which is expected to lead to an improved determination of the CKM matrix element $|V_{cb}|$.

We thank the KEKB group for the excellent operation of the accelerator, the KEK cryogenics group for the efficient operation of the solenoid, and the KEK computer group and the National Institute of Informatics for valuable computing and Super-SINET network

support. We acknowledge support from the Ministry of Education, Culture, Sports, Science, and Technology of Japan and the Japan Society for the Promotion of Science; the Australian Research Council and the Australian Department of Education, Science and Training; the National Science Foundation of China under contract No. 10175071; the Department of Science and Technology of India; the BK21 program of the Ministry of Education of Korea and the CHEP SRC program of the Korea Science and Engineering Foundation; the Polish State Committee for Scientific Research under contract No. 2P03B 01324; the Ministry of Science and Technology of the Russian Federation; the Ministry of Higher Education, Science and Technology of the Republic of Slovenia; the Swiss National Science Foundation; the National Science Council and the Ministry of Education of Taiwan; and the U.S. Department of Energy.

[1] P. Gambino and N. Uraltsev, Eur. Phys. J. **C 34**, 181 (2004).
[2] C.W. Bauer, Z. Ligeti, M. Luke, A.V. Manohar, Phys. Rev. **D67** (2003), 054012.
[3] A. Falk and M. Luke, Phys. Rev. **D 57**, 424 (1998).
[4] A. Falk, M. Luke and M. Savage, Phys. Rev. **D 53**, 2491 (1996); *ibid*, **53**, 6316 (1996).
[5] J. Abdallah, *et al.* (DELPHI Collab.), submitted to Eur. Phys. J. (CERN-EP-PH/2005-015).
[6] S.E. Csorna, *et al.* (CLEO Collab.), Phys. Rev. **D70**, 032002 (2004).
[7] B. Aubert, *et al.* (BABAR Collab.), Phys. Rev. **D69**, 111104 (2004).
[8] M. Voloshin and M. Shifman, Sov. J. Nucl. Phys. **45**, 292 (1987); J. Chay, H. Georgi and B. Grinstein, Phys. Lett. **B 247**, 399 (1990); I. Bigi, N. Uraltsev and A. Vainshtein, Phys. Lett. **B 293**, 430 (1992).
[9] M. Kobayashi and T. Maskawa, Prog. Theor. Phys. **49**, 652 (1973).
[10] A. Abashian *et al.* (Belle Collaboration), Nucl. Instr. and Meth. **A 479**, 117 (2002).
[11] S. Kurokawa and E. Kikutani, Nucl. Instr. and Meth. **A 499**, 1 (2003), and other papers included in this volume.
[12] R. Brun *et al.*, GEANT 3.21, CERN Report DD/EE/84-1 (1984).
[13] J. Duboscq *et al.* (CLEO Collaboration), Phys. Rev. Lett. **76**, 3898 (1996).
[14] N. Isgur and D. Scora, Phys. Rev. **D 52**, 2783 (1995). See also N. Isgur *et al.*, Phys. Rev. **D 39**, 799 (1989).
[15] J.L. Goity and W. Roberts, Phys. Rev. **D 51**, 3459 (1995).
[16] E. Barberio and Z. Was, Comp. Phys. Comm. **79**, 291 (1994).
[17] The selection of hadronic events is described in K. Abe *et al.* (Belle Collaboration), Phys. Rev. **D 64**, 072001 (2001).
[18] Throughout this paper, the inclusion of the charge conjugate mode is implied.
[19] K. Hanagaki *et al.*, Nucl. Instr. and Meth. **A 485**, 490 (2002).
[20] A. Abashian *et al.*, Nucl. Instr. and Meth. **A 491**, 69 (2002).
[21] Throughout this paper, quantities calculated in the B meson rest frame are denoted by an asterisk.
[22] A. Höcker and V. Kartvelishvili, Nucl. Instr. Meth. **A372**, 469 (1996).
[23] S. Eidelman *et al.*, Phys. Lett. **B592**, 1 (2004).